

INVERSE PRE-DEFORMATION OF FINITE ELEMENT MESH FOR LARGE DEFORMATION ANALYSIS

Arbtip Dheeravongkit and Kenji Shimada*
Carnegie Mellon University

ABSTRACT

In the finite element analysis that deals with large deformation, the process usually produces distorted elements at the later stages of the analysis. These distorted elements lead to analysis problems, such as inaccurate solutions, slow convergence and premature termination of the analysis. This paper proposes a new mesh generation algorithm to mesh the input part for pure Lagrangian analysis, where our goal is to improve the shape quality of the elements during the analysis in order to reduce the number of inverted elements as well as to decrease the chance of premature termination of the analysis. One pre-analysis is required to collect the geometric information and stress information in the analysis. The proposed method then uses the deformed shape boundary known from the pre-analysis, finds the optimal node locations, considers the stress information to control the mesh sizes as well as control the mesh directionality, generates meshes on the deformed boundary, and finally, maps the elements back to the undeformed boundary using inverse bilinear mapping. The proposed method has been tested on two forging example problems. The results indicate that the method can improve the shape quality of the elements during the analysis, and consequently extend the life of the analysis, which reducing the chance of premature analysis termination.

Keywords: Large Deformation Analysis, Mesh generation, Inverse Pre-deformation, Bubble Mesh

1. INTRODUCTION

The process of finite element analysis that deals with large deformation usually produces distorted elements at the later stages of the analysis. These distorted elements lead to several problems; inaccurate results, slow convergence and premature analysis termination.

Metal-forming processes are the most common applications involved with large deformation analysis; they include forging, extrusion, rolling, deep drawing, and so on. This paper will stress the problem of two-dimensional closed-die forging.

Two examples of two-dimensional closed-die forging, shown in Figure 1 are examined in this paper. The setting of each problem consists of a rigid die moving downward at a constant velocity onto the deformable part, which is constrained on the left and bottom edges. The die deforms the part into geometry with sharp corners, which eventually produce highly distorted elements during the analysis. As the finite element analysis is made on these problems using pure Lagrangian method, several elements experience severe distortion. Consequently, the analysis of the first example cannot be completed, and the results of the second example contain many ill-shaped elements.

Although there are two conventional techniques, adaptive remeshing and Arbitrary Lagrangian-Eulerian (ALE), for addressing this problem, both techniques have drawbacks. The adaptive remeshing technique completely remeshes the part at every certain number of analysis steps [1-3], however, the drawback of this method is its high computational costs [3]. The other solution is an analysis type called Arbitrary Lagrangian-Eulerian (ALE), which is the combination of Lagrangian and Eulerian analysis. It was developed to reduce the repetition of complete remeshing [4-8]. However, because of its complexity, the computation cost is much more expensive than using pure Lagrangian analysis. There are also some limitations, since in many cases ALE analysis cannot prevent the need for complete remeshing, and remapping of state variables is another drawback of this method [4].

As an alternative solution, this paper proposes a method to pre-deform an input mesh for Lagrangian analysis; the goal is to improve the shape quality of the elements during analysis in order to reduce the number of inverted elements, and to reduce the chance of premature analysis termination.

The remainder of the paper is organized as following: Section 2 discusses two existing methods used in the finite element analysis of large deformation processes. Section 3 discusses the proposed method. Results are shown in section 4 and Section 5 is the Conclusion.

* Correspondence to: Kenji Shimada
The Department of Mechanical Engineering, Carnegie Mellon University
5000 Forbes Avenue, Pittsburgh, PA 15213, Email: Shimada@cmu.edu

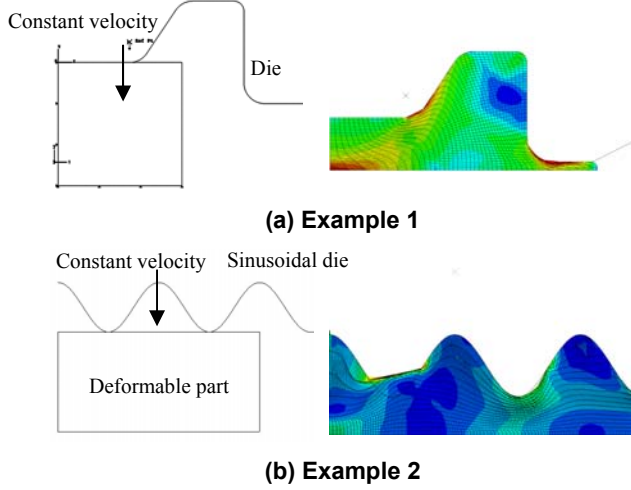


Figure 1: Example of large deformation finite element analysis of closed-die forging

2. PREVIOUS METHODS

2.1 Adaptive Remeshing

Adaptive remeshing is a method for enriching the mesh domain whenever it becomes unacceptable due to severe distortion during the analysis process. The general concept is to replace old and unsuitable mesh with a new and better-conditioned mesh when the error approximation of the analysis exceeds the tolerance, or the maximum error value allowed [2]. The newly created mesh may not necessarily have the same topology as the old mesh, and the number of nodes and elements of the new mesh may differ from the old mesh. Therefore, the state variables and history-dependent variables must also be transferred from the old to the new mesh. State variables include nodal displacements and the variables of the contact algorithm. The history-dependent variables are the stress tensor, strain tensor, plastic strain tensor, and so on.

Adaptive remeshing procedures can be summarized in the following four steps [1, 2, 3]:

Step 1: Determine the error estimator to define remeshing criterion

Because remeshing must be performed when a specified tolerant error is exceeded [2], the error estimator or error indicator must then be determined. The error indicator is defined by the strain error in L_2 norm, where the error $\|e_\varepsilon\|_\tau$ for an element τ is given by:

$$\begin{aligned} \|e_\varepsilon\|_\tau &= \left(\int_{\Omega} (\varepsilon - \varepsilon_h)^2 d\Omega \right)^{1/2} \\ \|e_\varepsilon\|_\tau &\approx \|e_\varepsilon^*\|_\tau = \left(\int_{\Omega} (\varepsilon^* - \varepsilon_h)^2 d\Omega \right)^{1/2} \end{aligned} \quad (1)$$

where ε and ε_h are the exact value and the finite element approximation of effective strain [1]. However, since the

value of ε is unknown, ε^* is then used to approximate the error instead, where ε^* is obtained by the recovery procedure.

In order to reduce the error, a remeshing criterion is then defined to achieve minimum percentage error [1]. The remeshing criterion is defined as:

$$\eta \leq \hat{\eta}$$

where

$$\eta = \frac{\|e_\varepsilon\|}{\|\varepsilon^*\|} \times 100\% \quad (2)$$

And $\hat{\eta}$ is the maximum relative percentage error allowed.

The error estimator is also used to control the mesh size field of new mesh to be regenerated. The mesh size field is necessary to reduce the geometric interference (the penetration) between the deformable part and the die surfaces, and to control mesh gradation [1].

Step 2: Remesh of the deformed body

In this step, the new and improved mesh is generated using several operations, including splitting, collapsing, and swapping of mesh edges and faces, and geometry modification of mesh vertices, edges or faces [1].

Step 3: Map the state variables and history dependent variables from the old to the new mesh

After generating a new mesh on the domain, the state variables and history-dependent variables are mapped from the old to the new mesh. For each node n in the new mesh, we have to determine which element in the old mesh it lies in, and map the variables of the old element onto the new mesh using the interpolation function [2]. To compute this procedure is very expensive; however, several methods have been developed which attempt to reduce the computational time in the mapping procedure, such as the “superconvergent patch recovery” method (SPR), by Zienkiewicz and Zhu [11, 12].

Step 4: Restart the simulation

Restart the simulation on the new generated mesh.

Because adaptive remeshing creates a new, more efficient mesh every time the specified error tolerance is exceeded, it could guarantee reasonably small error and solve the geometric distortion of the mesh during analysis. The disadvantage of this technique is its high computational cost especially during the procedure of determining the error estimator and mapping variables from an old to a new mesh. More importantly, computational costs increase considerably in analysis of more complicated geometries. The challenge of this technique, therefore, is to find an optimal mesh with the minimum number of nodes (unknowns), within a constraint, so that the finite element error does not exceed the specified limit, and computational costs are minimized. Furthermore, applying local

modification, instead of remeshing the entire domain also reduces the computational costs significantly [1].

2.2 Arbitrary Lagrangian-Eulerian (ALE)

The Arbitrary Lagrangian-Eulerian (ALE) method is another technique for handling the large deformation problem in finite element analysis. This method basically combines the features of pure Lagrangian analysis and Eulerian analysis, two common types of finite element analysis. The concepts of Lagrangian analysis, Eulerian analysis and ALE method are as follows:

Lagrangian analysis

In this type of analysis, mesh follows the deformation of the material during analysis, in other words, the mesh is connected to the material throughout the finite element calculation [5]. When performing finite element analysis of this type, the deformation path is approximated by increments in time; in each increment, the history of the material is taken into account as the initial condition for the next increment [4]. Since the mesh and the material are connected, severe distortion of the mesh can cause difficulty in the finite element calculation. It is here that adaptive remeshing must be applied to improve the shape quality of the mesh in order to continue the analysis.

Eulerian analysis

In contrast to Lagrangian analysis, the elements in Eulerian analysis are not deformed, because the mesh and the material are not connected. Instead, the mesh is fixed to a spatial coordinate system while the material flows during the simulation [4, 5]. This method is commonly used in fluid mechanics. Because there is no connection between the mesh and the material, it is more difficult to determine the history of the material. This causes the process of mapping variables in Eulerian analysis, called “Advection”, computationally expensive. Another problem of this type of analysis is that it is difficult to obtain an accurate description of the free surface.

Arbitrary Lagrangian-Eulerian

ALE is a method that combines the previous two types of analysis. In the ALE method, the mesh is neither connected to the material nor fixed to a spatial coordinate system. However, it is prescribed in an arbitrary manner [4]. During the analysis, the mesh elements deform according to the Lagrangian method, however, instead of repositioning the nodes at their original position and performing advection, as in the Eulerian method, the nodes are placed at other positions to obtain optimal mesh quality. The mesh nodes have velocity associated with them in order to obtain the updated mesh. Mesh velocity plays an important role in the ALE method, as it reduces the analysis error, and prevents mesh distortion [4]. Another important characteristic of this method is that it changes the location of the nodes in the existing mesh, instead of creating a completely new mesh like the adaptive remeshing method, and it maintains the same (or similar) mesh topology throughout the analysis [5].

In conclusion, ALE is a Lagrangian analysis that takes advantage of the advection techniques of Eulerian analysis. The ALE method is more powerful than either the Lagrangian or the Eulerian method. However, because of its complexity, it is more computationally expensive than other types of analysis. Nevertheless, the main objective of this method is to reduce the number of complete adaptive remeshing required in the analysis and to lessen some computational costs.

There are additional limitations in ALE analysis. In many cases the mesh suffers considerable distortion, and the same mesh topology cannot be held for the entire analysis. In such cases, complete adaptive remeshing is still required. Another drawback of ALE is the state-variables remapping step, which is much more complicated than in the Lagrangian method. Moreover, unless the remapping process is performed very accurately, the history of the material will not be properly understood [4].

3. THE PROPOSED METHOD

As an alternative solution, a new mesh pre-deformation method is proposed here, to mesh the input part for Lagrangian analysis and improve the shape quality of the elements during analysis, in order to reduce the number of inverted elements and decrease the possibility of premature analysis termination.

The method can be summarized in the following four steps:

- (1) Pre-Analysis:** Run a pre-analysis on a simple uniform mesh to collect the node locations and stress information regarding the deformed part.
- (2) Bubble Mesh Packing:** Find the optimal node locations inside the deformed boundary using Bubble Mesh [13-17]. Use the stress information obtained from Step 1 to control the size of elements, and use the boundary information to control the directionality of the mesh. Then generate a new mesh on the deformed boundary.
- (3) Inverse Bilinear Mapping:** Use inverse bilinear mapping [9, 10] to map the node locations from the deformed boundary to the undeformed boundary.
- (4) Full Analysis:** Run the actual analysis on the new pre-deformed mesh.

The general concept behind this method is that the deformation behavior of the elements is predicted first from the initial analysis. Then information from the analysis is used to inversely map the new node locations generated by the Bubble Mesh [13-17] from the deformed boundary onto the initial boundary in order to generate input mesh for the real analysis. As a result, the pre-deformed mesh elements in the initial boundary would have the approximately inverse shape of the mesh elements in the deformed part of the pre-analysis. Figure 2 illustrates the overview of the proposed algorithm. The goal of this algorithm is to reduce the number of elements which are severely distorted, as well as to reduce the chance of premature termination of the analysis. Next, we will discuss each step of the algorithm in detail.

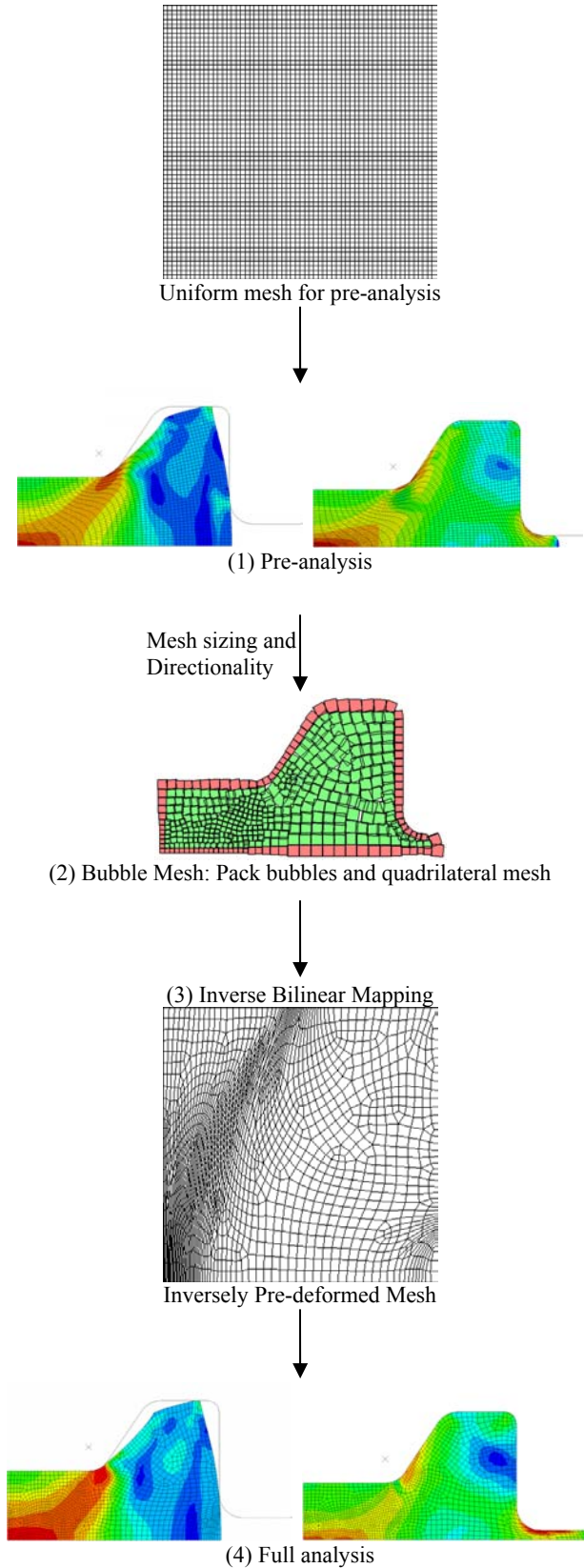


Figure 2: Overview of the proposed method

3.1 Pre-Analysis

The work presented in this paper can be achieved using any finite element package. For this paper, ABAQUS has been used to run the analysis. Followings are the models of the two example problems we considered in this paper:

Example 1

The model of this problem consists of a rigid die and a deformable blank. The blank is 0.3m by 0.3m and has 60×60 elements, with Young's modulus of elasticity of 100GPa, Poisson's ratio of 0.3, and initial yield stress of 200MPa. The geometry of the die is shown in Figure 3.

The die moves downward on to the deformable blank with a constant velocity 0.2m/s, while the blank is constrained along the left and the bottom sides.

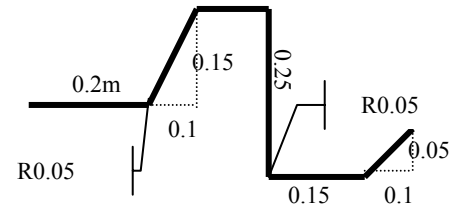


Figure 3: Die geometry of example 1

Example 2 [18]

The model consists of a rigid die and a 20mm by 10mm deformable blank. The die has a sinusoidal shape with amplitude and period of 5 and 10 mm, respectively. The blank is steel and modeled as a von Mises elastic-plastic material with a Young's modulus of 200 GPa, an initial yield stress of 100 MPa, and a constant hardening slope of 300 MPa. Poisson's ratio is 0.3; the density is 7800 kg/m³. The die is moved downward vertically at a velocity of 2000 mm/sec and is constrained in all other degrees of freedom.

From analysis of these models, the results give the boundary shape of the deformed blank and stress information, which will be used in the later steps. Pre-analysis is carried out until severe distortion occurs, or when 50%-80% of the actual analysis is completed because we only want to predict the deformation behavior of the problem.

3.2 Bubble Mesh

In this step, we use the boundary of the deformed blank obtained from pre-analysis in the first step; square bubbles are packed inside the boundary and a new, all-quadrilateral mesh is generated. Details of Bubble Mesh algorithm can be found in [13-17].

When generating the new input mesh, the size of element should be properly determined. Ideally, smaller elements are desired around the sharp-corner regions, where they tend to experience more distortion. For this reason, we use stress information collected from pre-analysis to control the size of elements through the tensor function of the Bubble

Mesh algorithm. Therefore, the new mesh has smaller elements around the sharp corners than elsewhere.

In addition to size control, directionality of the mesh is also considered. Since boundary information is known, the directionality of the new mesh can be controlled to align with the boundary.

The result of this step is a new graded quadrilateral mesh inside the pre-analysis deformed boundary. Figures 5 (1a-1c) and (2a-2c) illustrate the bubble packing processes with size and directionality controls for Examples 1 and 2 respectively.

3.3 Inverse Bilinear Mapping

After optimal node locations have been located inside the pre-analysis deformed boundary, we can now map the new node locations back to the initial boundary. To achieve this, we have to use the relation between the old node locations in the initial boundary and the new node locations in the deformed boundary, then apply inverse bilinear mapping [9, 10].

Let (x,y) be the coordinate of the source space and (u,v) be the coordinate of the destination space.

$$x = auv + bu + cv + d, \text{ and} \quad (3)$$

$$y = euv + fu + gv + h, \quad (4)$$

where a, b, c, d, e, f, g and h are constants. Solving for v in Equation 3, then substituting in Equation 4, we obtain:

$$(au + c)(fu + h - y) - (eu + g)(bu + d - x) = 0, \text{ or}$$

$$Au^2 + Bu + C = 0. \quad (5)$$

Similarly, solving for u in the Equation 4, then substituting in the Equation 3, we obtain:

$$(av + b)(gu + h - y) - (ev + f)(cu + d - x) = 0, \text{ or}$$

$$Dv^2 + Ev + F = 0. \quad (6)$$

Equation 5 gives two solutions, and Equation 6 gives another set of two solutions.

$$u = \frac{-B \pm \sqrt{B^2 - 4AC}}{2A}, \quad v = \frac{x - bu - d}{au + c}$$

$$v = \frac{-E \pm \sqrt{E^2 - 4DF}}{2D}, \quad u = \frac{y - bv - h}{ev + f}$$

However, since only one unique solution is valid for the range of $0 \leq u \leq 1$ and $0 \leq v \leq 1$, we obtain a unique solution.

In summary, we first have to find out, in the deformed boundary, which old element e_i that each new node n_i lies in. Next we can calculate the u and v vectors that give the location of this new node n_i inside the old element e_i . Then the inverse bilinear mapping can be performed to map this

new node from the deformed boundary to the undeformed boundary using the calculated vector u and v as shown in Figure 4.

The result of this step is a new pre-deformed mesh inside the initial boundary. Figure 5-1d and 5-2d show the resultant pre-deformed mesh.

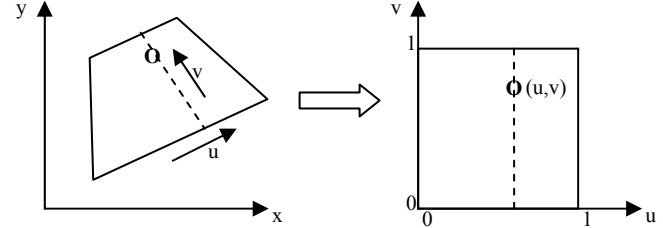


Figure 4: Inverse Bilinear Mapping

3.4 Full Analysis

Run the full analysis on the new pre-deformed mesh obtained from the previous step on ABAQUS.

4. RESULTS AND DISCUSSION

In this section, the results from the analysis of the pre-deformed mesh are shown and compared with the results from the analysis of the original uniform mesh. To illustrate the importance of mesh size control and mesh directionality control, we will also compare the analysis results of three different pre-deformed meshes: (1) Uniform sized pre-deformed mesh, (2) Pre-deformed mesh with size control, and (3) Pre-deformed mesh with size and directionality controls. Since two examples are examined in this paper, each example will be examined individually. In each example, we will do the followings:

- Compare the results of the original uniform mesh and the pre-deformed mesh
- Show the importance of mesh size control. (Compare the results of pre-deformed mesh with and without mesh size control)
- Show the importance of directionality control. (Compare the results of pre-deformed mesh with mesh size control only and mesh with both size and directionality controls)

Example 1

a) Compare the results of the original uniform mesh and the pre-deformed mesh

Figures 6 and 7 illustrate the analysis results of the original mesh, uniform-sized pre-deformed mesh (mesh without size or directionality control), pre-deformed mesh with mesh size control, and pre-deformed mesh with size and directionality controls respectively. By comparing maximum step time these analyses can carry out, it is apparent that the pre-deformed mesh could carry the analysis to further step than the original mesh, although less than half the number of nodes in the original mesh was used. The results are summarized in Table 1.

Furthermore, the maximum numbers of frames of the analyses can be used to compare how quickly the results converge. As shown in Table 1, the analysis of the original mesh used 332 frames to reach maximum step time of 0.898, while the pre-deformed meshes require fewer numbers of frames to reach the greater maximum step time. This comparison implies that the pre-deformed meshes have larger step time increments and tend to converge faster than the original mesh.

Table 1: Comparing maximum time and number of frames of the original and pre-deformed meshes

	Numbers of Nodes	Max step time	Max # of frames
Mesh 1-a	1681	0.9018	275
Mesh 1-b	1587	0.9235	279
Mesh 1-c	1723	0.9217	307
Mesh 1-d	1661	0.9221	267

- (a) Original mesh
- (b) Uniformed-sized pre-deformed mesh
- (c) Pre-deformed mesh with size control
- (d) Pre-deformed Mesh with size and directionality control

b) The importance of the graded mesh.

It is demonstrated in Figures 6 and 7 that the thin elements, which we generate intentionally at the locations expected to encounter the sharp corner during analysis, are gradually unfolded as the analysis is continuing. Consequently, the shapes of the elements tend to be progressively improved as performing the analysis. However, when comparing the last frames of both analyses, as shown in Figure 8, it is shown there are yet some bad elements around the sharp corner of the pre-deformed mesh without the size control (Figure 8a). However, this problem can be solved when applying the mesh size control to yield smaller elements around the sharp corner, as shown in Figure 8b.

c) The importance of the directionality control.

The close look at another sharp corner on the right side of the deformed blank can illustrate the importance of the directionality control as shown in Figure 9. It is obviously shown in the figure, that with the mesh directionality controlled, we can significantly improve the shape of the elements in the result mesh. This is because when we generate the input mesh, we try to align the elements with the boundary. Therefore, when we run analysis on that input mesh, as the analysis is continuing, thin elements are unfold along the moving boundary, which reducing the chance of producing inverted elements.

Example 2

a) Compare the results of the original uniform mesh and the results of the pre-deformed mesh

Figures 10 to 11 illustrate the analysis results of the original mesh, uniform sized pre-deformed mesh (Mesh without any size or directionality control), pre-deformed mesh with mesh size control, and pre-deformed mesh with size and directionality controls respectively. In this example, we do not encounter the early termination in the analysis of any case. However, the results at the later stages of all analyses

contain many undesired bad shaped elements. Therefore, for this example, we compare the step time when each analysis start producing inverted elements. The results are summarized in the Table 2 below.

According to the results shown in Table 2 above, the pre-deformed mesh can effectively improve the results by extending the time before the analysis start producing inverted elements.

Table 2: Comparing the step time when each analysis start producing inverted elements

	Number of Nodes	Step time start producing inverted elements
Mesh 2-a	2718	1.368E-4
Mesh 2-b	2533	1.672E-4
Mesh 2-c	2517	3.420E-4
Mesh 2-d	2585	3.344E-4

- (a) Original Mesh
- (b) Uniform Sized Pre-deformed Mesh
- (c) Pre-deformed Mesh with size control
- (d) Pre-deformed Mesh with size and directionality control

b), c) The importance of the size and directionality control.

By comparing the step time each analysis start producing inverted elements in Table 2, it is shown that the pre-deform mesh with size and directionality control give better results than the pre-deformed mesh with uniform mesh size. Moreover, by comparing the element shape in the result mesh at the step time where we take the boundary to generate new input mesh using bubble packing (Step time = 1.5E-04) as shown in Figure 12, it is apparent that mesh size and directionality control improve the shape of the elements around the two sharp corners significantly.

5. CONCLUSION

According to the results shown in the previous section, four important points can be concluded

1. The pre-deformed mesh can carry out the analysis to further step than the original mesh, which implies that the pre-deformed mesh can reduce the chance of early termination of the analysis.
2. The pre-deformed mesh tends to converge faster with larger step increment. This will save the time completing the analysis.
3. The mesh size control can solve the unwanted large angles in elements around the sharp corner.
4. The mesh directionality control can improve the element shape around the sharp corner.

ACKNOWLEDGEMENT

The first author acknowledges a graduate fellowship provided by Thai Government

This material is based in part on work supported under a NSF CAREER award (No. 9985288).

REFERENCES

- [1] Jie Wan, Suleyman Kocak and Mark S. Shephard, "Automated Adaptive Forming Simulations," *Proceedings, 12th International Meshing Roundtable*, Sandia National Laboratories, pp.323-334, 2003.
- [2] Timo Meinders, "Simulation of Sheet Metal Forming Processes," Chapter 5. Adaptive Remeshing, Canada, 1999.
- [3] Amir R. Khoei and Roland W. Lewis, "Adaptive Finite Element Remeshing in a Large Deformation Analysis of Metal Powder Forming," *International Journal for Numerical Methods in Engineering* 45, pp. 801-820, 1999.
- [4] Christiaan Stoker, "Developments of Arbitrary Lagrangian-Eulerian Method in Non-Linear Solid Mechanics, Applications to Forming Processes," *University of Twente*, ISBN 90-36512646, 1999.
- [5] Abaqus 6.3 Explicit User Manual, Chapter 7.6 Adaptive Meshing.
- [6] M'hamed Souli, Lars Olovsson and Ian Do, "Ale and Fluid-Structure Interaction Capabilities in Ls-Dyna," 7th International Ls-Dyna Users Conference, 2002.
- [7] M'hamed Souli and Lars Olovsson, "Ale and Fluid-Structure Interaction Capabilities in Ls-Dyna", 2002.
- [8] M'hamed Souli, "An Eulerian and Fluid-Structure Coupling Algorithm in Ls-Dyna," 1999.
- [9] Jonas Gomes, Lucia Darsa, Bruno Costa and Luiz Velho, "Warping and Morphing of Graphical Objects," Chapter3: Transformation of Graphical Objects.
- [10] Paul Heckbert, "Fundamental of Texture Mapping and Shading," Chapter 2: Two-Dimensional Mappings.
- [11] Zienkiewicz Oc and Zhu Jz, "The Super-convergent Patch Recovery and a Posteriori Error Estimates, Part1: The Recovery Technique," *International Journal for Numerical Methods in Engineering*, 1992.
- [12] Zienkiewicz Oc and Zhu Jz, "The Super-convergent Patch Recovery and a Posteriori Error Estimates, Part2: Error Estimates and Adaptivity," *International Journal for Numerical Methods in Engineering*, 1992.
- [13] Kenji Shimada and David C. Gossard, "Bubble Mesh: Automated Triangular Meshing of Non-Manifold Geometry by Sphere Packing," *Proceedings of The Third ACM Symposium on Solid Modeling and Applications*, pp. 409-419, 1995.
- [14] Kenji Shimada, Atsushi Yamada, and Takayuki Itoh, "Anisotropic Triangular Meshing of Parametric Surfaces via Close Packing of Ellipsoidal Bubbles," *6th International Meshing Roundtable, Sandia National Laboratories*, pp. 375-390, 1997.
- [15] Soji Yamakawa and Kenji Shimada, "High Quality Anisotropic Tetrahedral Mesh Generation via Ellipsoidal Bubble Packing," *Proceedings, 9th International Meshing Roundtable, Sandia National Laboratories*, pp. 263-273, 2000.
- [16] Kenji Shimada, Jia-Huei Liao and Takayuki Itoh, "Quadrilateral Meshing with Directionality Control through the Packing of Square Cells," *Proceedings, 7th International Meshing Roundtable, Sandia National Lab*, pp. 61-76, 1998.
- [17] Naveen Viswanath, "Adaptive Anisotropic Quadrilateral Mesh Generation Applied to Surface Approximation," MS Thesis, *Carnegie Mellon University*, 2000.
- [18] Abaqus Example Problems Manual Version 6.3, Section 1.3.9 Forging with Sinusoidal Die.

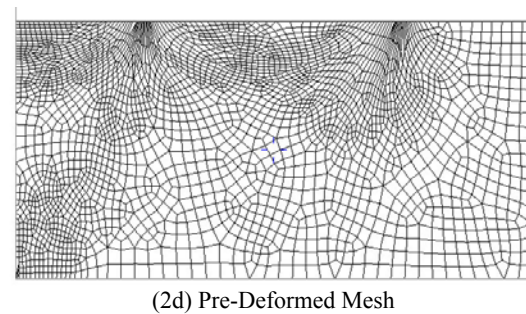
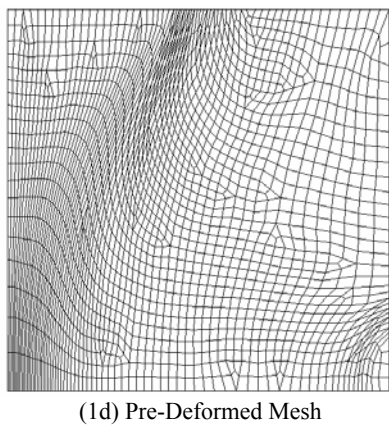
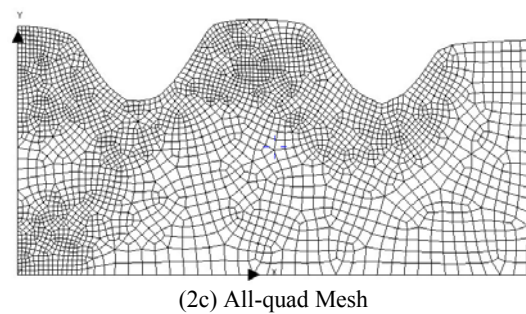
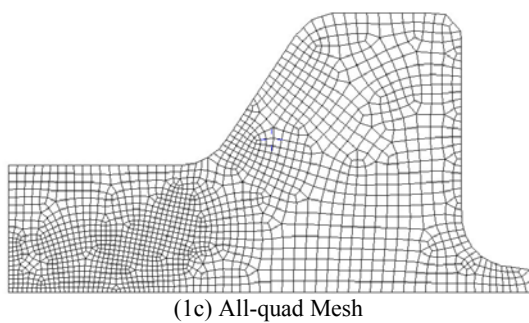
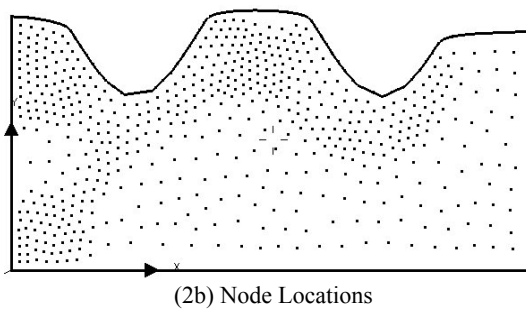
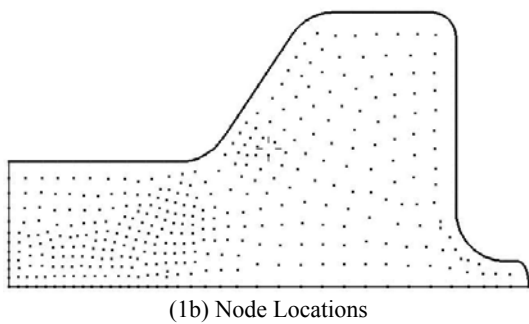
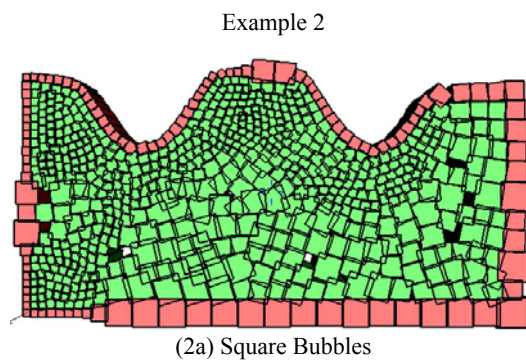
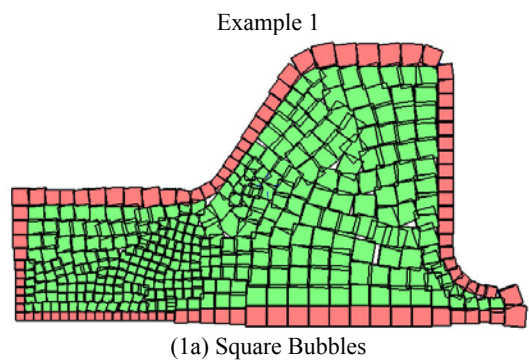


Figure 5: Quadrilateral Bubble Mesh Packing and resultant pre-deform mesh for Examples 1 and 2

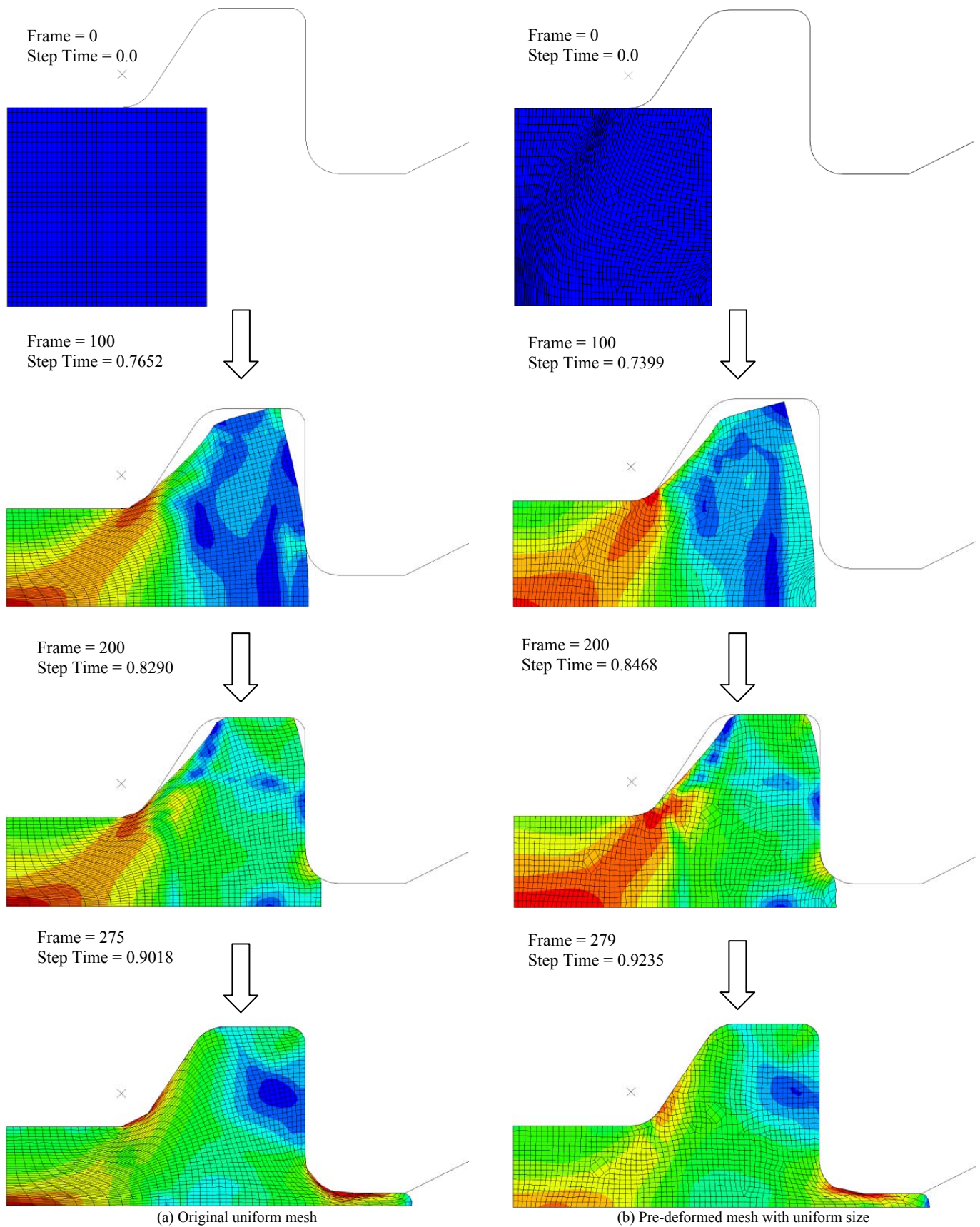
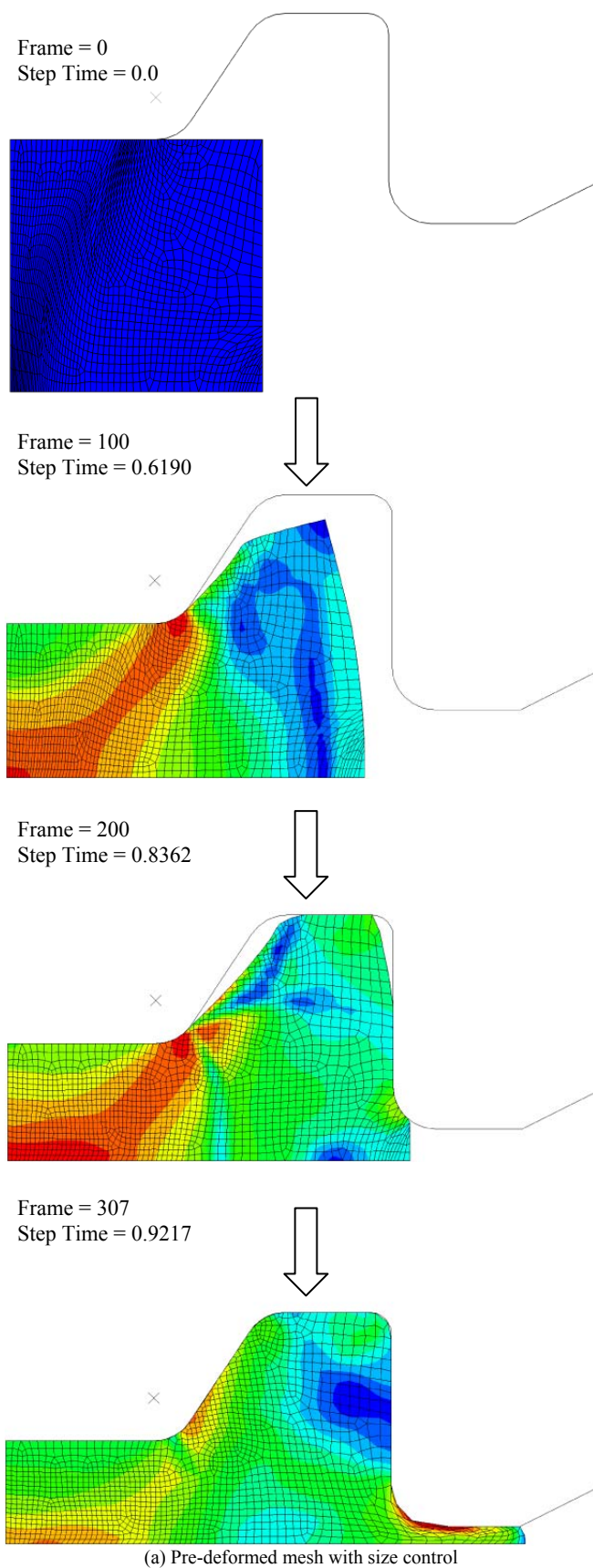
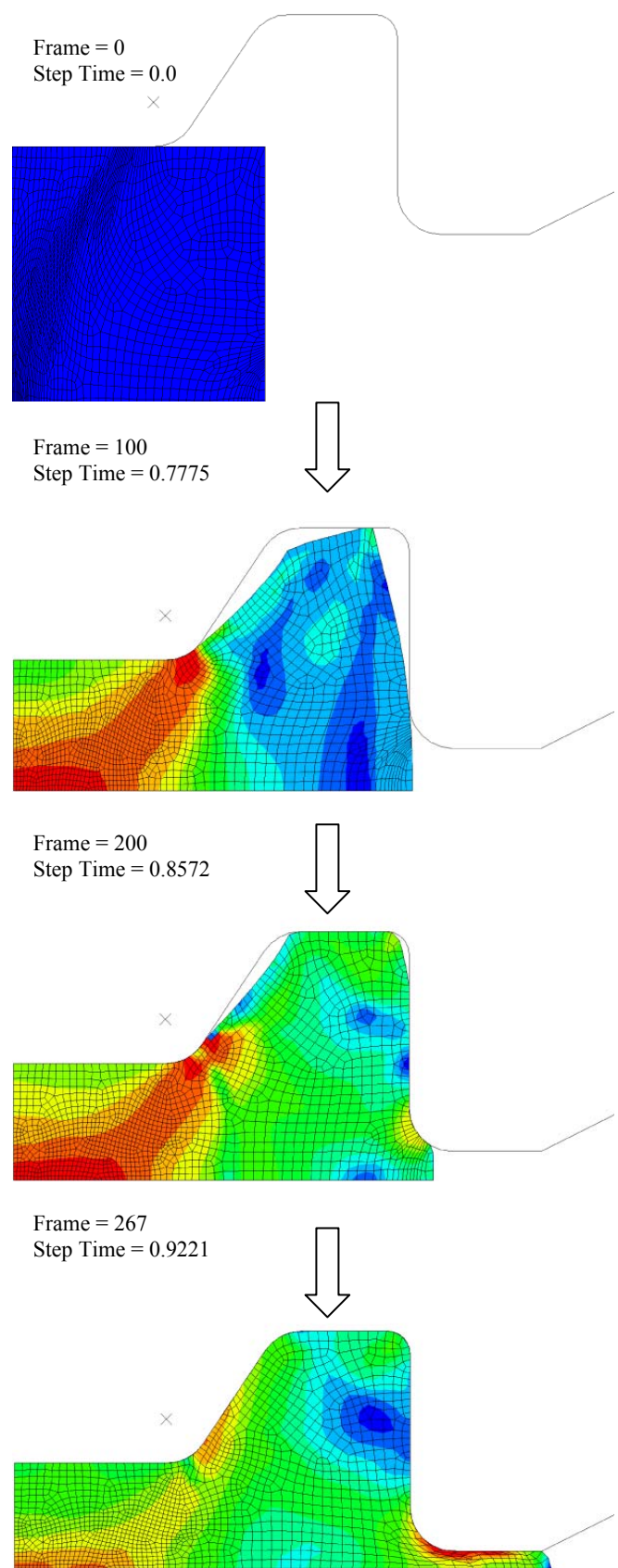


Figure 6: Finite element analysis of the original uniform mesh (a) and the uniform sized pre-deformed mesh (b) (Example1)

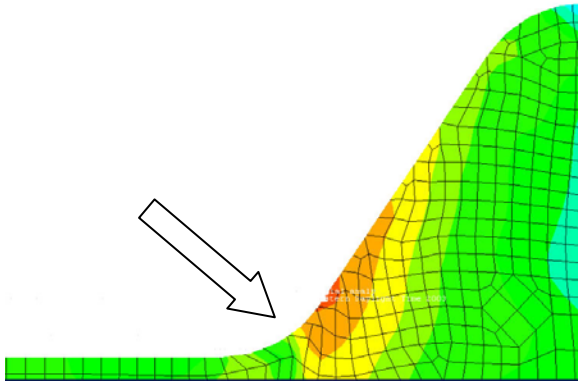


(a) Pre-deformed mesh with size control

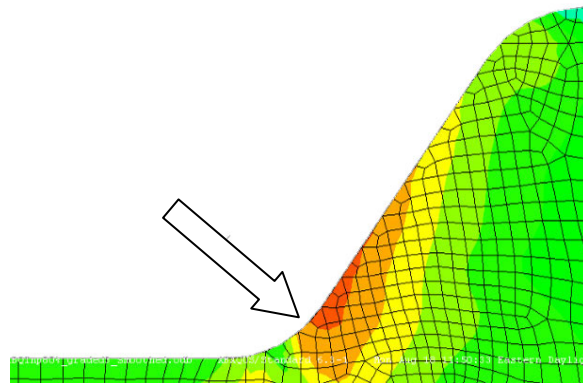


(b) Pre-deformed mesh with size and directionality controls

Figure 7: Finite element analysis of the pre-deformed mesh with size control (a) and the pre-deformed mesh with size and directionality controls (b) (Example1)

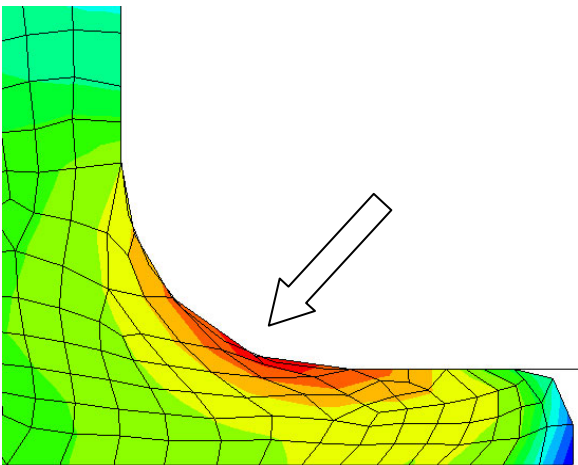


(a) The result of pre-deformed mesh without mesh size control

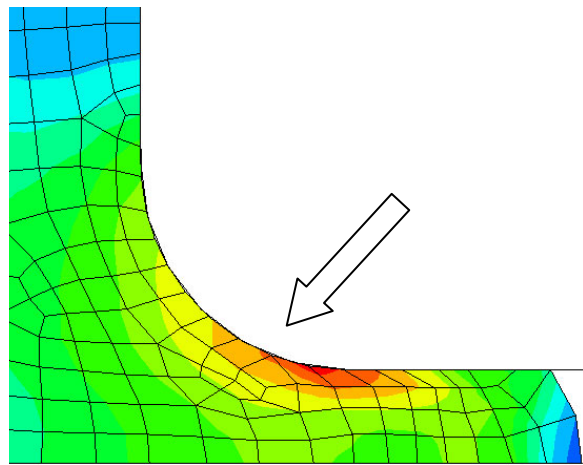


(b) The result of pre-deformed mesh with mesh size control

Figure 8: Comparing the sharp corner of the results of pre-deformed mesh with and without mesh size control

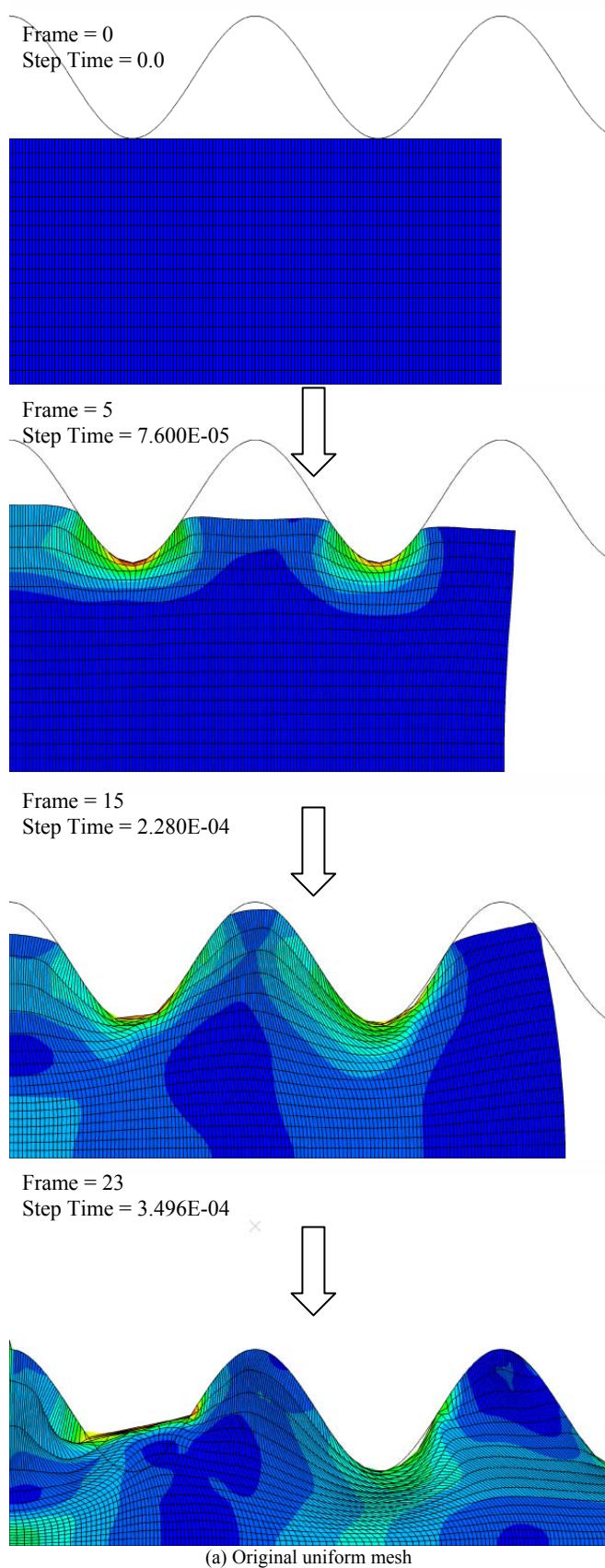


(a) The result of Pre-deformed mesh without directionality control

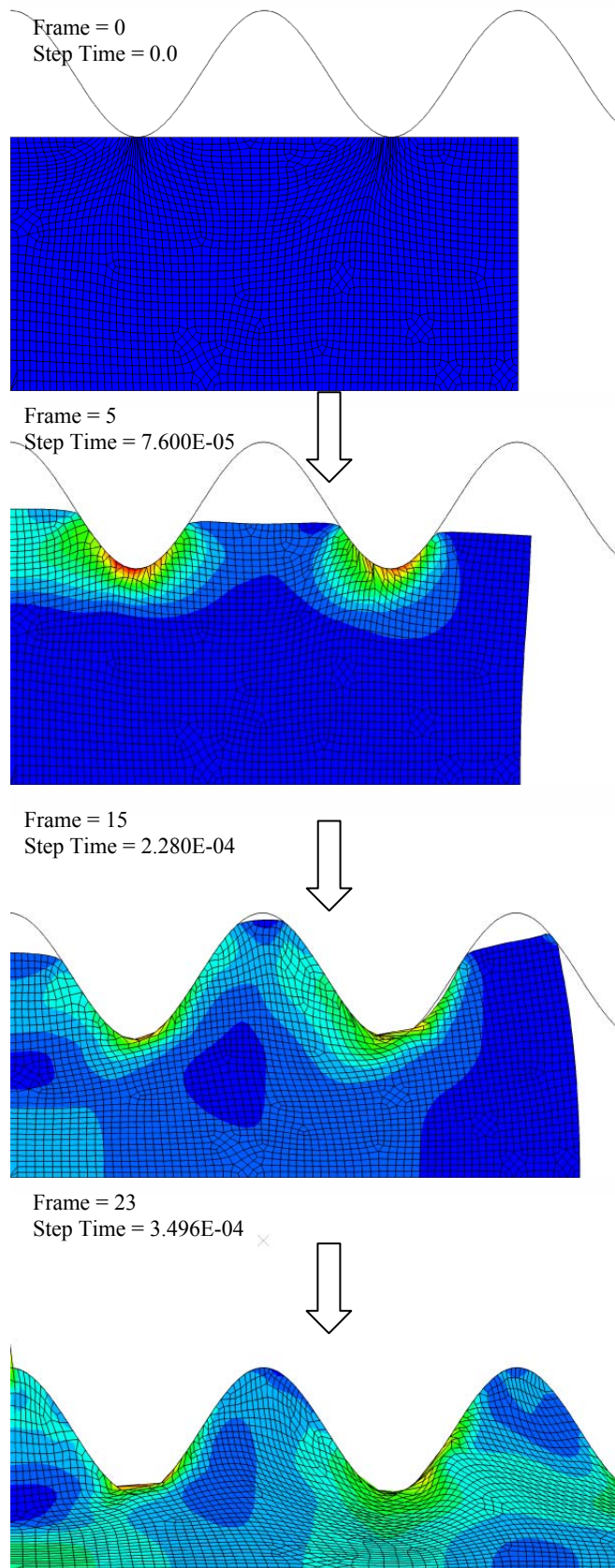


(b) The result of Pre-deformed mesh with directionality control

Figure 9: Comparing the sharp corner of the results of pre-deformed mesh with and without mesh directionality control

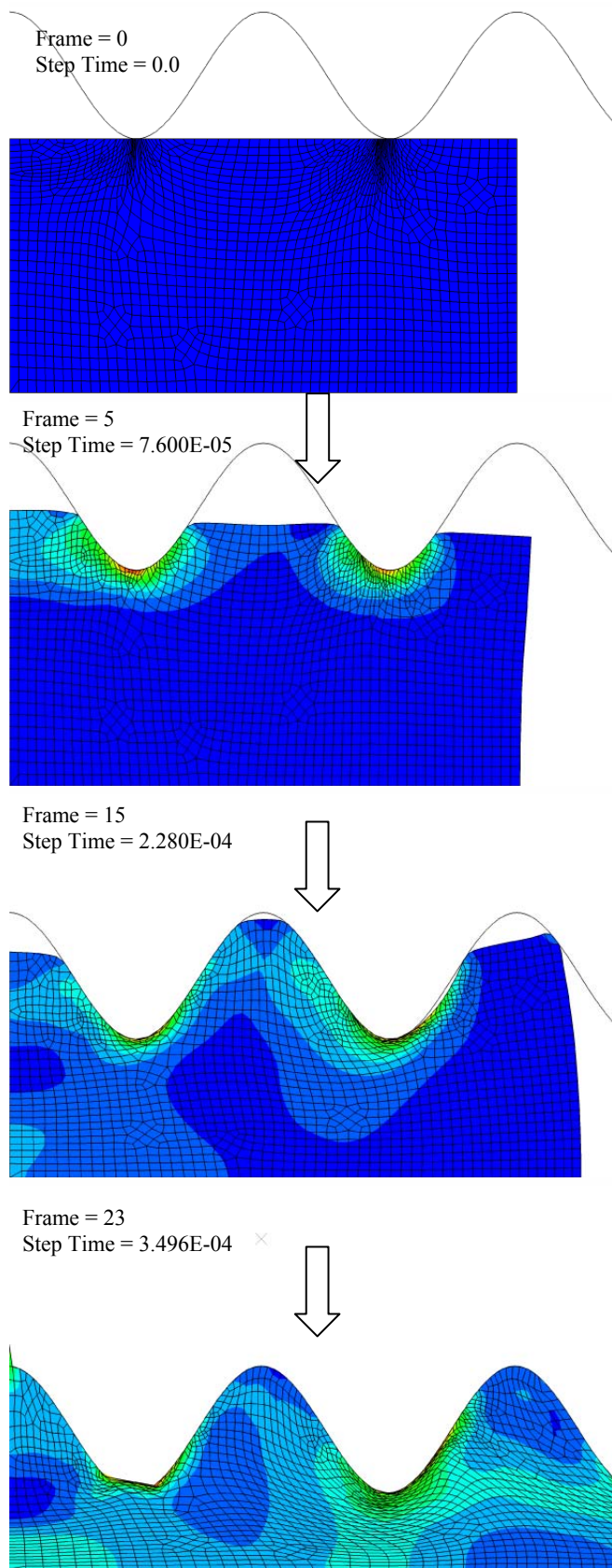


(a) Original uniform mesh

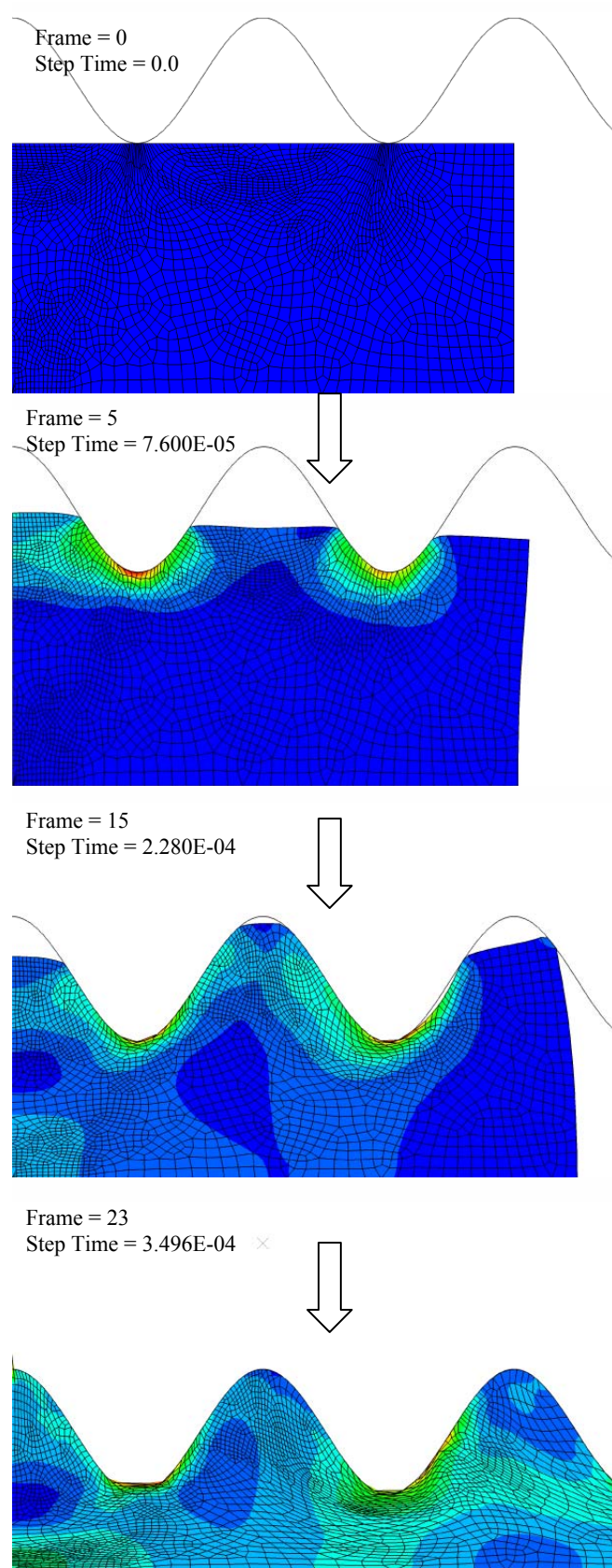


(b) Pre-deformed mesh with uniform size

Figure 10: Finite element analysis of the original uniform mesh (a) and the uniform sized pre-deformed mesh (b) (Example2)

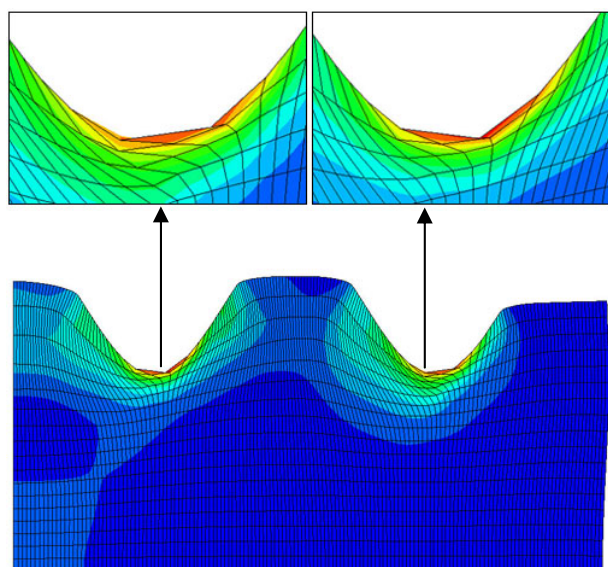


(a) Pre-deformed mesh with size control

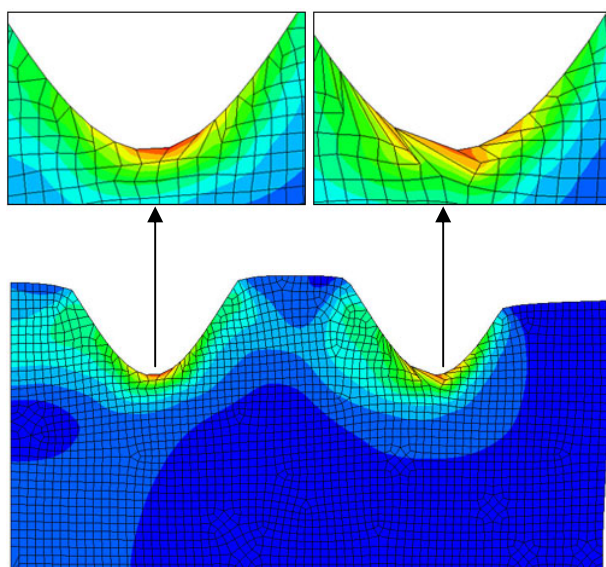


(b) Pre-deformed mesh with size and directionality controls

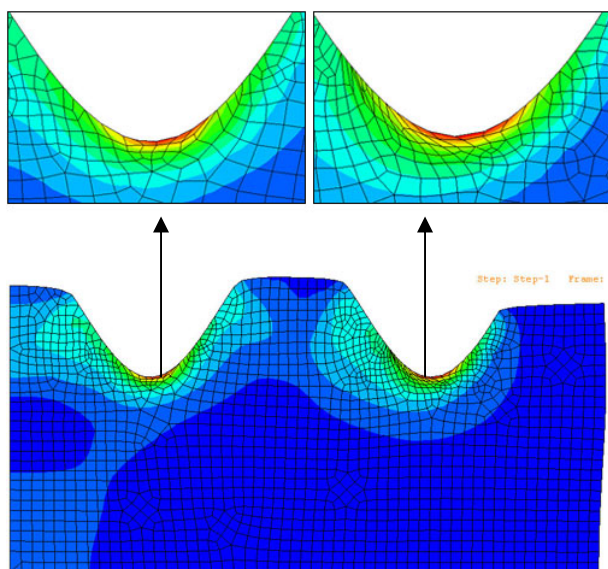
Figure 11: Finite element analysis of the pre-deformed mesh with size control (a) and the pre-deformed mesh with size and directionality controls (b) (Example2)



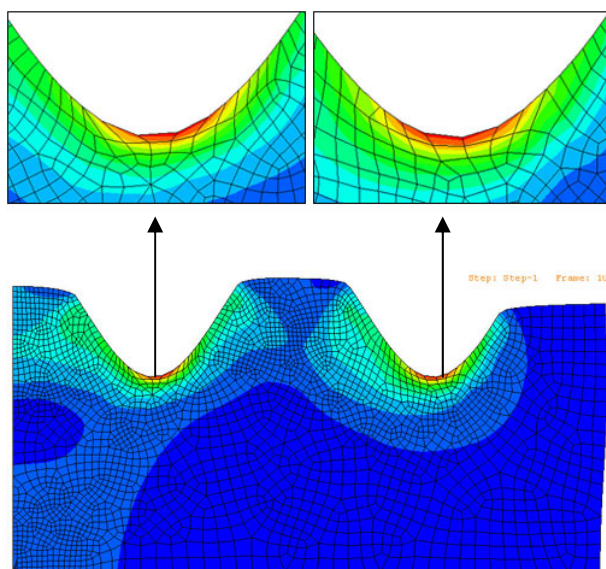
(a) Original Mesh



(b) Uniform sized Mesh



(c) Mesh with size control



(d) Mesh with size and directionality control

Figure 12: Result mesh at the step time where the boundary was taken to generate the new input mesh